Scientia Iranica D (2023) 30(3), 1127–1138

Sharif University of Technology
Scientia Iranica
Transactions D: Computer Science & Engineering and Electrical Engineering
http://scientiairanica.sharif.edu

Design optimization of coreless stator axial flux-switching motor

H. Asgharpour-Alamdari*

Department of Electrical Engineering, Technical and Vocational University (TVU), Tehran, P.O. Box 14357-61137, Iran.

Received 9 May 2021; received in revised form 23 June 2021; accepted 23 August 2021

KEYWORDS
Finite element method;
Axial field flux-switching permanent magnet motor;
Coreless;
Optimization, Taguchi method.

Abstract. This study aims to provide an analytical design, optimization, and Three-Dimensional (3D) simulation through Finite Element Method (FEM) of a coreless stator Axial Field Flux-Switching Motor (AFFSM). The motor consists of two indented rotors with a coreless stator between them containing a magnet and winding. First, the electrical and magnetic design of the motor was developed, and the values of its basic parameters were calculated. Then, machine optimization was evaluated using the Taguchi algorithm in order to minimize the motor cogging torque. Some of the basic motor dimensions such as the magnet length and width, rotor tooth width and height, and back iron thickness were selected as the optimization variables, and the best combination of these variables was obtained by changing them in a certain range to achieve the desired objective. Then, the accuracy of the analytical design and optimization was evaluated by forming a 3D FEM of the motor and investigating its performance. A comparison of the optimized and primary motors revealed that the optimal design exhibited a better performance than its initial counterpart. Finally, a prototype of the proposed motor was fabricated and tested, indicating that the experimental results were largely similar to the analytical results.

1. Introduction

Considering the power density, higher efficiency, and low rotor losses, Axial Flux Permanent Magnet Machines (AFPMMs) proved to be greatly advantageous over traditional Radial Flux Permanent Magnet Machines (RFPMMs) [1]. The AFPMMs can be divided into two major categories namely the internal rotor AFPMMs and internal stator AFPMMs. While the single rotor in the former is between two stators, that in the latter is between two rotors. More developments were executed on the internal stator AFPMMs for high performance applications. The Yokeless-And-Segmented-Armature (YASA) AFPMMs are distinct among the internal stator AFPMMs owing to their design, which distinguish them for their modular stator topology, hence better performance as a result of short-end windings, higher fill factor, and absence of stator core [2,3].

As already mentioned, compared to the application of RFPMMs, AFPMMs will be notably advantageous. Furthermore, given the high torque density as well as the more compact structure of the axial flux machines [4,5], the AFPMMs are better suited for applications with high space limitation. They are widely used in wind turbine applications [6], flywheel energy storage systems, Electric Vehicle (EV), and hybrid vehicles [7].

*. *Tel.: +981132312902*
E-mail address: asgharpour_alamdari@tvu.ac.ir (H. Asgharpour-Alamdari)

doi: 10.24200/sci.2021.58284.5652

Considerable attention has been recently paid to Axial Field Flux-Switching Permanent Magnet (AFFSPM) machines. The AFFSPM machines enjoy both advantages of the AFPMMs and those of flux-switching machines [8], thus presenting a machine with a short axial length that makes it compact and robust and also, with a high power density on top of other advantages [9,10].

As previously mentioned, in the AFPMMs with coreless stator topologies, loss of the stator will overcome the iron losses, thus eventually adding to its advantages. In addition, removal of the stator core losses ensures higher efficiency in the coreless stator AFPM as a result of which a smaller motor stack is obtained. Moreover, in the absence of the stator core in these machines, the reluctance variation is eliminated, which leads to the abolition of the cogging torque. On the contrary, in the absence of stator core, the AFPMM needs to use more permanent magnets to overcome the core difficulties to produce the same magnetic flux density in the air gap.

The Taguchi method is an optimization method initially developed by Dr. Genichi Taguchi in the 40 s at the Japanese Electrical Communications Laboratories. The motivation behind the development of this optimization was the realization that using judicious planning would drastically reduce the cost of development [11].

In the literature, the Taguchi method has been frequently applied to various types of electrical machines such as brushless DC PM motors [12,13], PM Synchronous Machines [14,15], line-start PMSM [16], induction machine [17], Reluctance Synchronous Machines or Switch Reluctance Machines [18,19], axial flux PM Synchronous Machines [20], linear or tubular machines [21,22], and superconducting wind generator [23].

Figure 1 introduces the novel AFPMM discussed in this paper. According to the observations, the stator of this motor is coreless containing coil and permanent magnet. As a result of the interaction between the permanent magnet and rotor teeth, cogging torque affects the proper performance of the motor. Therefore, this paper primarily aims to reduce the cogging torque using the Taguchi method.

The paper is structured as follows. Section 2 shows the AFFSPM motor characteristics and design process. Section 3 investigates the machine optimization and simulation based on the Taguchi method and transient magnetic time-stepping Finite Element-Method (FEM). Section 4 presents experimental results and finally, Section 5 concludes the study.

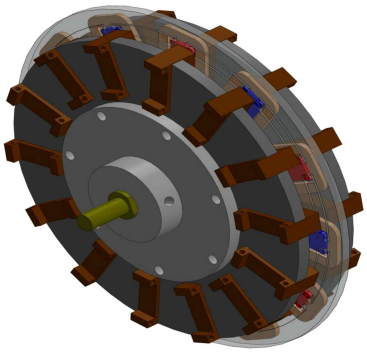

Figure 1. Proposed AFSPMM.

2. Sizing equations

Figures 1 and 2 illustrate the structure of the coreless stator flux-switching motor proposed in this paper. According to these figures, the stator is coreless that consists of 12 non-overlapping coils with rectangular magnets placed in them. Further, two rotors with 14 teeth are located at the top and bottom of the stator. At any given time, some rotor teeth are placed in front of the stator permanent magnets with opposite magnetization direction, as shown in Figure 3, and the coil flux linkage is switched and voltage is induced in each coil. The proposed motor specifications are listed in Table 1.

The design of the AFFSPM motor is very similar to those of the coreless stator and double-rotor AFPMMs [24,25]. In the conventional coreless stator AFPMMs, the magnets are placed on the rotor and the stator coils are located between the two rotor cores. In the structure proposed in this article, the rotor consists of tooth instead of PM, the coil and

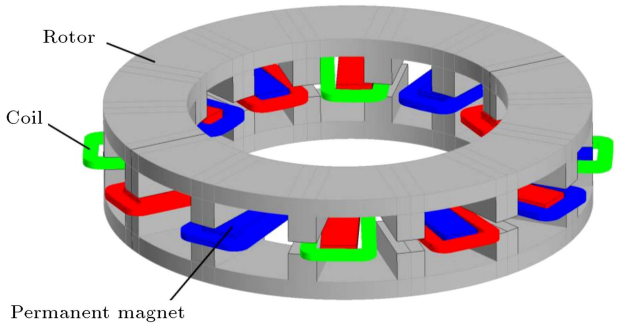

Figure 2. Rotor, stator, and coil.

Table 1. Proposed motor characteristics.

Output power	Number of stator magnets	Number of rotor pole pairs	Rated speed	Rated frequency
1000 W	12	14	1500 RPM	350 HZ

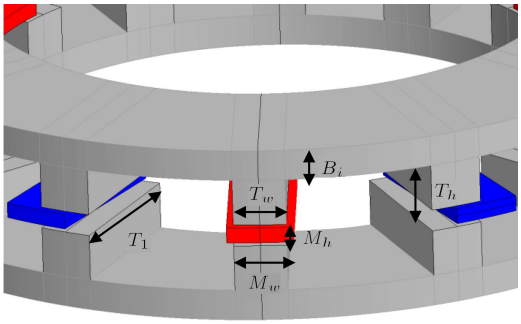

Figure 3. Permanent magnets and rotor position.

magnets are located in the stator, and the magnet is surrounded by the coil. In the case of conventional axial flux motors, the outer diameter is calculated in Eq. (1) where α_p, A_c, k_w, w_s, B_{mg}, η, $\cos(\varphi)$, and λ are the ratio of the magnet width to pole pitch, electrical loading, winding factor, rated speed (rpm), maximum air gap flux density (T), efficiency, power factor, and ratio of the inner to outer diameter motor, respectively. In addition, for the coreless stator, the AFPM value is equal to 0.955 [23]. The number of turns per phase and maximum magnetic flux per pole can be defined through Eqs. (2) and (3) [26], where E_f is the rms of no-load Back-EMF (V), f the frequency (Hz), N_c the number of coil turn, and $\phi_{\max}$ (Wb) maximum magnetic flux per pole [27]. The frequency of the Back-EMF is calculated through Eq. (4) where N_r is the number of rotor teeth and w_s is the rotor speed in rpm.

$$D_{out} = \sqrt[3]{\frac{32P_{out}}{\pi^3\alpha_p A_c K_w w_s B_{mg}(1-\lambda^2)(1+\lambda)\cos(\varphi)}}, \quad (1)$$

$$N_c = \frac{E_f}{\pi\sqrt{2}fK_w\varphi_{\max}}, \quad (2)$$

$$\phi_{\max} = B_{mg}A_p = B_{mg}\alpha_p\frac{\pi}{8N_r}(1-\lambda^2)D_{out}^2, \quad (3)$$

$$f = \frac{N_r w_s}{60}. \quad (4)$$

3. Optimization and FEM analysis

3.1. Optimization

Cogging torque generally occurs due to the difference between the magnetic reluctance at the permanent magnet in the stator as well as the rotor teeth. The cogging torque in PM machines causes noise and vibration; therefore, it is necessary to reduce it as much as possible in the design stage. In this regard, the goal of the optimization is to reduce the peak of cogging torque in the AFFSPM motor. The cogging torque is reduced based on the assumption that the optimized motor torque is not less than the initial motor torque.

Figure 4 depicts the flowchart of the Taguchi method steps. First, based on this figure, the objective

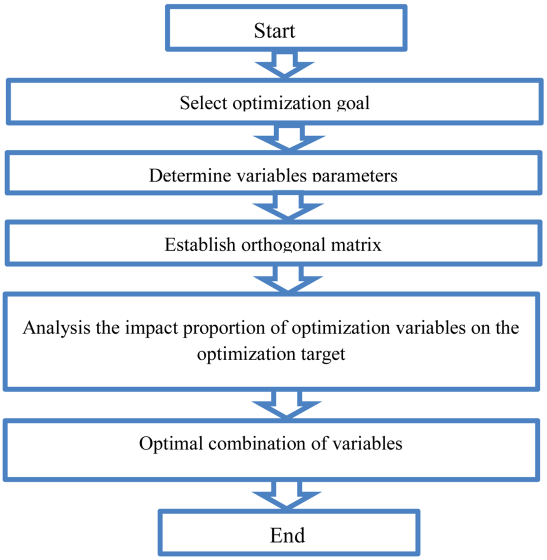

Figure 4. Taguchi method process.

of optimization is determined. Then, the optimization variables are selected, and the level of their changes is identified. Next, according to the variables and number of levels of their changes, the table of Taguchi experiments is plotted and the results of each experiment are extracted using the FEM.

Once the simulations are completed, maximum cogging torque and torque are calculated for each experiment, and the most suitable combination is selected according to the results.

3.1.1. Determine the optimization variables

The optimization parameters are defined as variables A, B, C, D, and E, and each parameter takes five factor levels. Here, A stands for the width of PM (M_w), B the height of the PM (M_h), C the height of rotor tooth (T_h), D the rotor tooth width (T_w), and E the rotor back iron height (B_i) (Figure 3). Table 2 lists the optimization variables and their levels.

3.1.2. Design and solve the orthogonal matrix of Taguchi experiment

Based on the five variables given in Table 2 that were selected for optimization and also the five-level factor ranges, the matrix of Taguchi experiments for each of the variables is given in Table 3. In case of conducting the traditional optimization experiments, the number of experiments would be $5^5 = 3125$; however, in the case of using the Taguchi optimization method, the number of the required experiments will be $5 \times 5 = 25$.

3.1.3. Analysis of mean value

To statistically analyze the results of the experiments, first, the average should be analyzed. The Taguchi optimization method uses this statical mean obtained from the orthogonal arrays according to the analysis results of the FEM given in Table 3. Eq. (5) shows

Table 2. Motor characteristics.

Variables	Level 1	Level 2	Level 3	Level 4	Level 5	Initial
A (M_w)	12	14	16	18	20	16
B (M_h)	5	6	7	8	9	7
C (T_h)	7	9	11	13	15	13
D (T_w)	10	12	14	16	18	12
E (B_i)	7	8	9	10	11	10

Table 3. Experimental arrays and results of FEM.

Experiment	*A*	*B*	*C*	*D*	*E*	$T_{cogging}$ (N.m)	Torque (N.m)
1	1	1	1	1	1	1.15	3.25
2	1	2	2	2	2	1	3.85
3	1	3	3	3	3	1.1	4.915
4	1	4	4	4	4	1.21	4.05
5	1	5	5	5	5	1.5	4.8
6	2	1	2	3	4	1.8	4.56
7	2	2	3	4	5	1.15	5.32
8	2	3	4	5	1	1.3	5.21
9	2	4	5	1	2	2.18	4.76
10	2	5	1	2	3	3	5.2885
11	3	1	3	5	2	1.8	5.4845
12	3	2	4	1	3	1.6	3.71
13	3	3	5	2	4	3.5	5.76
14	3	4	1	3	5	1.4	4.5255
15	3	5	2	4	1	1.15	6.28
16	4	1	4	2	5	1.2	5.09
17	4	2	5	3	1	1.65	4.76
18	4	3	1	4	2	0.65	5.5
19	4	4	2	5	3	2.3	5.8
20	4	5	3	1	4	1.4	5.4
21	5	1	5	4	3	0.9	6.2
22	5	2	1	5	4	1.35	5.5
23	5	3	2	1	5	1	4.905
24	5	4	3	2	1	1.1	5.9
25	5	5	4	3	2	1.05	5.33

Table 4. Average values of all experiments.

Parameter	$T_{cogging}$ (N.m)	Torque (N.m)
Average value	1.599	5

the average calculation formula, and Table 4 lists the obtained results:

$$M = \frac{1}{n}\sum_{i=1}^{n} S_i. \tag{5}$$

The average of each factor level is calculated in (6):

$$b_{xi} = \frac{1}{5}(b_x(j) + b_x(l) + b_x(m) + b_x(k) + b_x(p)), \tag{6}$$

where b_{xi} defines the average value of the factor x at the level of ith, b_x indicates the index of target performance under some experiment of the parameter x, and parameters j, k, m, l, and p represent the experimental numbers. For instance, the average value of the peak cogging torque of factor D at Level 2 is calculated as follows:

$$b_{D2} = \frac{1}{5}(b_D(2) + b_D(10) + b_D(13) + b_D(16) + b_D(24)). \tag{7}$$

Table 5. Experimental arrays and results of FEM

Variables	Level of each factor	$T_{cogging}$ (N.m)	Torque (N.m)
	1	1.252	4.213
	2	1.886	5.0277
A	3	1.93	5.152
	4	1.44	5.31
	5	1.08	5.567
	1	1.37	5.1
	2	1.35	4.628
B	3	1.51	5.258
	4	1.678	5.0071
	5	1.68	5.3125
	1	1.55	4.8128
	2	1.45	5.079
C	3	1.31	5.4039
	4	1.272	4.678
	5	2.006	5.296
	1	1.466	4.405
	2	1.96	5.1777
D	3	1.44	4.8181
	4	1.012	5.47
	5	1.71	5.3989
	1	1.27	5.08
	2	1.336	4.9849
E	3	1.78	5.1827
	4	1.852	5.054
	5	1.25	4.9681

The average values for all variable levels can be calculated, similarly. Table 5 as well as Figures 5 and 6 present the analysis results.

3.1.4. Analyzing the impact of the proportion of the optimization variables on the optimization

To assess the relatively important design variables based on the analysis results and find their best combination, as seen in Eq. (8), Analysis of Variance (ANOVA) was employed. In Eq. (8), x denotes different variables (A, B, C, D, and E), i the levels of those variables (from 1 to 5), P the motor performance, Maximum cogging torque ($T_{cogging}$ (N.m)), Average Torque (Torque (N.m)), $L_{x_i}(P_j)$ the performance average value given in Table 4, and $L_{x_i}(P_{x_i})$ the performance average value at each level of factor variable shown in Table 5. Table 6 represents the Sum of Squares (SS) as well as

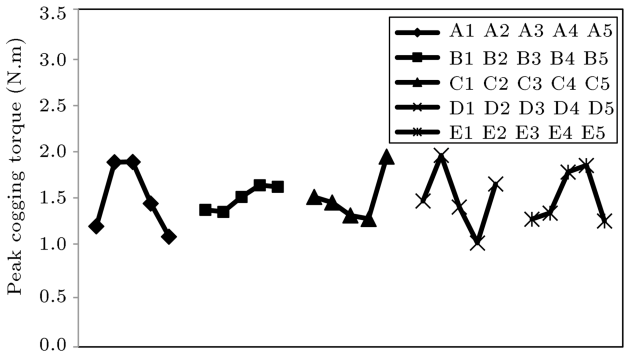

Figure 5. Main factor effects on motor cogging torque.

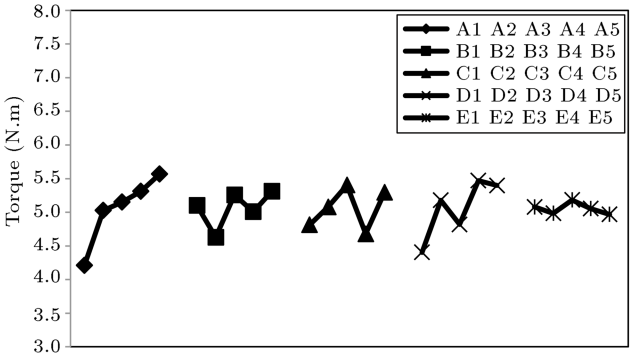

Figure 6. Main factor effects on motor average torque.

the proportion results.

$$SS = 5\sum_{i=1}^{5}\sum_{j=1}^{2}\left[L_{(x_i)}\left(P_{(x_i)}\right) - L_{(x_i)}(P_j)\right]^2. \quad (8)$$

3.1.5. Using RSM to determine the optimal combination of variables

As mentioned earlier, the aim of optimization is to minimize $T_{cogging}$ and maximize *Torque*. The Response Surface Methodology (RSM) is used to attain the best combination of factors. The interactions of factors with specific responses are also investigated. In an optimization study, factors are the variables chosen to identify the best combination of factors. Furthermore, responses represent key indicators that are affected by chosen factors. RSM creates a set of experiments or simulation runs to assess the responses based on the factors chosen. The following equation is a general second-order model for RSM:

$$y = c_0 + \sum_{i=1}^{n_f} c_i f_i + \sum_{i=1}^{n_f} c_{ii} f_i^2 + \sum_{i<j=2} \sum^{n_f} c_{ij} f_i f_j, \quad (9)$$

where y represents the considered response, f the selected factor, n_f the number of factors, and c's the unknown coefficients obtained through regression analysis. This research aims to optimize two responses at the same time. A technique known as the desirability function was then used to simultaneously optimize

Table 6. Proportion of impacts caused by various factors on motor performance.

Variables	$T_{cogging}$ (N.m)		Torque (N.m)	
	SS	Proportion (%)	SS	Proportion (%)
A	1.046	41.27	0.6958	34.64
B	0.29	11.6	0.0443	2.21
C	0.381	15.03	0.2803	13.95
D	0.7841	30.94	0.5944	29.59
E	0.0293	1.16	0.3939	19.61
Total	**2.54**	**100**	**2**	**100**

more than one response. As the desirability function approaches one, the response meets the optimal solution.

As previously shown in Table 2, five independent variables were chosen as the optimization factors. For the selected factors, RSM suggests 32 simulation runs based on the central composite design approach. Finally, the RSM calculations were done in MINITAB software, and the mathematical model was employed to estimate the behavior of each response. The designed experiments and performed simulation runs are reported in Table 7. Moreover, the results of the second-order model for $T_{cogging}$ and *Torque* are presented in Eqs. (10) and (11), respectively:

$$\begin{aligned} T_{cogging} =& 53.5 + 0.538A - 2.94B - 0.183C \\ & - 3.612D - 4.47E - 0.0290A \times A \\ & - 0.0173B \times B - 0.0058C \times C \\ & + 0.0672D \times D + 0.0331E \times E \\ & - 0.0093A \times B - 0.0011A \times C \\ & + 0.0185A \times D + 0.0279A \times E \\ & + 0.0583B \times C + 0.0443B \times D \\ & + 0.2416B \times E - 0.0058C \times D \\ & + 0.0034C \times E + 0.1196D \times E, \end{aligned} \tag{10}$$

$$\begin{aligned} Torque =& -31.0 + 0.58A + 2.25B + 1.95C \\ & + 0.90D + 0.50E + 0.0001A \times A \\ & - 0.109B \times B + 0.0143C \times C \\ & + 0.0066D \times D + 0.113E \times E \\ & + 0.0516A \times B - 0.0164A \times C \\ & - 0.0071A \times D - 0.0474A \times E \\ & - 0.0487B \times C - 0.0536B \times D \\ & - 0.018B \times E - 0.0305C \times D \\ & - 0.1216C \times E - 0.0145D \times E. \end{aligned} \tag{11}$$

By using the RSM model and desirability functions, an optimal combination of the factors reflecting the optimal solution was obtained, the results of which are given in Table 8. The composite desirability of the optimal suggestion was measured as 0.967.

Table 9 lists the anticipated value of each response as well as the confirmation run used to calculate the RSM error. As shown in this table, based on the optimal combination values reported in Table 8 ($A = 20$, $B = 5.13$, $C = 14.5$, $D = 13.64$, and $E = 11$), RSM predicts the response values of $T_{cogging}$ and Torque as 0.65 N.m and 5.67 N.m, respectively. The confirmation run for the optimal combination was then carried out, and the values for $T_{cogging}$ and Torque are obtained as 0.7 N.m and 5.5 N.m. As shown in Table 9, the error of the RSM prediction is less than 5%, thus confirming the validity of the RSM application to this optimization problem. As presented in Table 9, the desirability values for $T_{cogging}$ and Torque were obtained as 0.939 and 0.996, respectively, which are close to the ideal condition.

3.2. FEM analysis of initial and optimized motors

The previous section investigated the desired motor optimization, and the best combination was selected to achieve the desired goal. To compare the performance of the primary and optimal motors in this section, Three-Dimensional (3D) analysis through the FEM was carried out. The specifications of the primary and optimal motors are given in Table 10 according to the variables included in the optimization section as well as the optimization results. Figure 7(a) and (b) present 3D views of the primary and optimized motors, respectively. A comparison of the magnet dimensions in both initial and optimal designs reveals that the volume of the permanent magnets of the optimal topology is about 11% less than that of the primary topology.

Table 7. Designed experiments using RSM and performed simulation runs.

Run number	Factors (variables)					Responses (objectives)	
	A (M_w)	B (M_h)	C (T_h)	D (T_w)	E (B_i)	$T_{cogging}$ (N.m)	Torque (N.m)
1	16	7	11	14	9	1.2	5
2	16	7	11	14	9	1.2	5
3	16	7	11	14	9	1.2	5
4	14	8	13	16	8	0.818	5.4
5	14	6	13	16	10	0.441	5.29
6	14	6	13	12	8	1.89	5.015
7	18	8	9	12	10	1.33	5.89
8	18	8	13	16	10	2.19	5.5759
9	16	7	11	14	9	0.91	4.9975
10	16	7	11	14	9	0.91	4.9975
11	14	8	13	12	10	1.82	4.7517
12	14	8	9	16	10	1.1571	5.485
13	14	6	9	16	8	0.41	4.93
14	16	7	11	18	9	2	5.93
15	18	6	9	16	10	0.88	6
16	18	8	9	16	8	0.52	6.3186
17	16	7	7	14	9	1.46	4.45
18	16	5	11	14	9	1.233	4.95
19	18	8	13	12	8	1.8	6.295
20	16	7	11	10	9	2.54	5.2
21	16	7	11	14	11	1.1	6.75
22	18	6	13	16	8	0.8	6.35
23	14	8	9	12	8	1.22	4.25
24	16	7	11	14	7	1.556	5.07275
25	16	9	11	14	9	1.02	5.1
26	18	6	13	12	10	1.118	5.08
27	18	6	9	12	8	1.745	4.757
28	20	7	11	14	9	0.77	6.6721
29	16	7	15	14	9	0.747	6.9265
30	16	7	11	14	9	0.874	6.778
31	12	7	11	14	9	0.694	4.25
32	14	6	9	12	10	0.68	4.41

Table 8. Optimal combination of factors.

Factors	Optimum value
$A(M_w)$	20
$B(M_h)$	5.13
$C(T_h)$	14.5
$D(T_w)$	15.64
$E(B_i)$	11

The magnetic flux density and flux path in the primary and optimized motors at the rated current and speed are shown in Figure 8. The maximum flux densities are almost 1.2 T in the yoke and teeth. The cogging torque in the primary and final motors is shown in Figure 9. As observed, the cogging torque in the optimized design is about 41% less than that of the primary design.

Figure 10 shows the motor three phase voltage in the no-load state at a rated speed. According to this figure, the peak voltage of the primary design and final design are about 86 and 92 V, respectively, with a 6 V difference.

In addition, Figure 11 shows the torque of the primary and optimal designs at a rated speed. According

Table 9. Response values attained for the optimal condition.

Response	Optimum results by RSM	Confirmation run	Error (%)	Desirability
$T_{cogging}$ (N.m)	0.67	0.7	4.28	0.939
Torque (N.m)	5.67	5.5	3.09	0.996

Table 10. Specifications of motors.

Parameter	Unit	Primary	Optimized
Rated power (P_{out})	W	1000	1000
Rated speed (w_s)	rpm	1500	1500
Number of phase (m)	—	3	3
Number of stator coils (Q_c)	—	12	12
Number of rotor tooth (N_r)	—	28	28
Rotor outer diameter (D_{out})	mm	270	270
Air gap Length (g)	mm	1.5	1.5
Ratio of inner to outer diameter (λ)	—	0.6	0.6
Magnet height (M_h)	mm	7	5.13
Magnet width (M_w)	mm	16	20
Number of turns per phase (N_{phase})	—	260	260
Magnet length (M_L)	mm	50	50
Tooth width (T_w)	mm	14	15.64
Tooth height (T_h)	mm	13	14.5
Tooth length (T_L)	mm	50	50
Back iron (B_i)	—	8	11
Magnet type	—	Neodymium iron boron: 42/15	Neodymium iron boron: 42/15

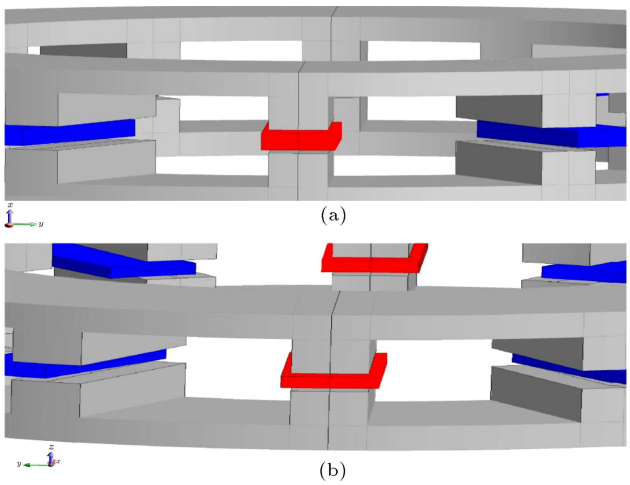

Figure 7. Initial and optimized motors.

to Figure 11, the torque curve of the optimal design has lower ripple than the original design due to the reduction of cogging torque.

4. Experimental results

In order to evaluate the accuracy of the analytical analysis of the previous sections, a prototype machine was created according to the results shown in Section 3. The final assembled motor is shown in Figure 12. No load test setup was built to measure the characteristics of the proposed motor. Cogging torque and Back-EMF test are the main parameters that are measured in the no-load test. The test setups of the measurement of the cogging torque and no-load phase voltage are shown in Figure 13(a) and (b), respectively. The method for cogging torque measurement was discussed in [28]. The stator was fixed to the jaws of a lathe machine and rotor rotate at a low speed. In this situation, a balanced beam was attached to the shaft and then, it was connected to the digital weight gauge. The torque was obtained from the reading of digital weight gauge. According to Figure 13(b), in the Back-EMF test, the motor shaft was connected to the lathe machine on

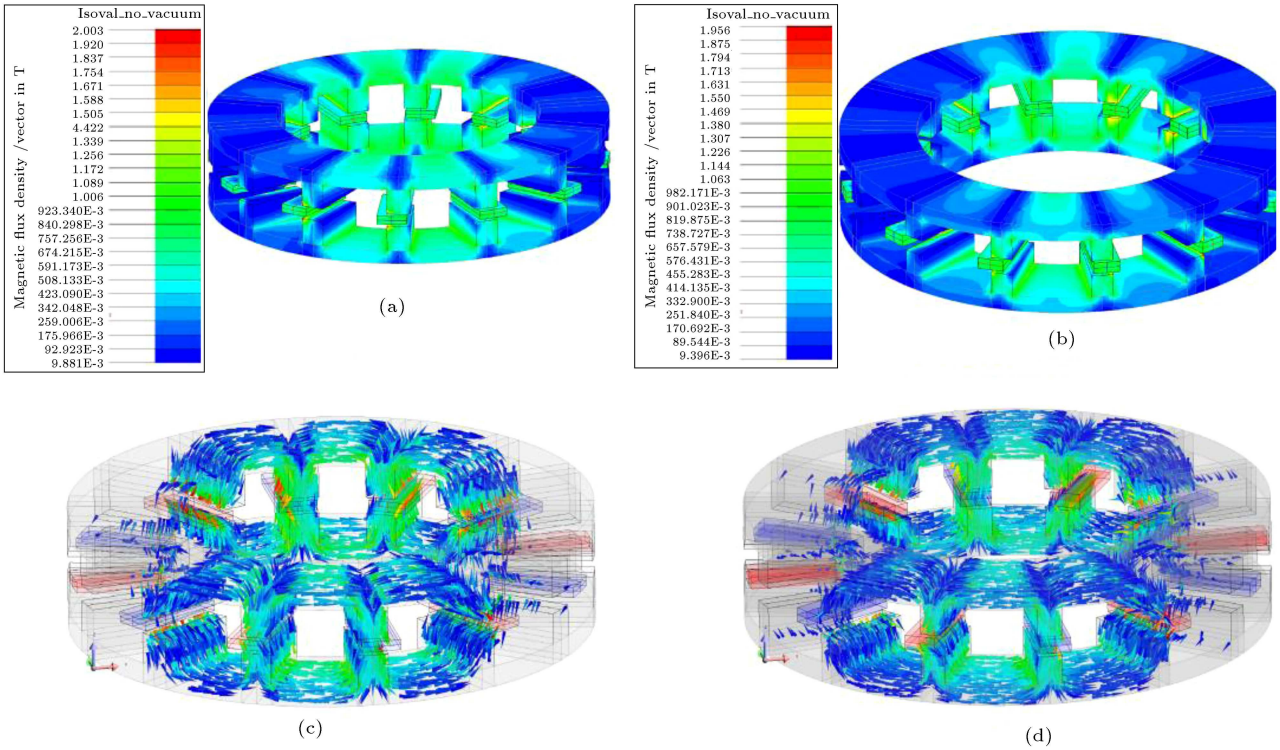

Figure 8. Flux density and flux path of two motors: (a) Flux density in optimized motor, (b) flux density in primary motor, (c) flux path in optimized motor, and (d) flux path in primary motor.

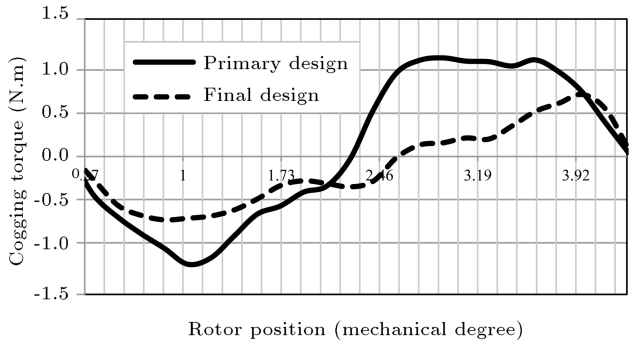

Figure 9. Cogging torque.

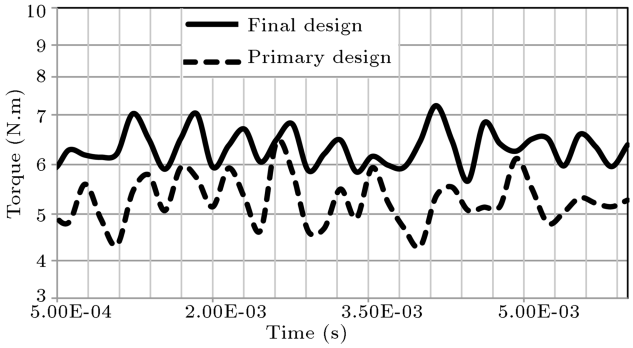

Figure 11. Torque at rated current and rated speed.

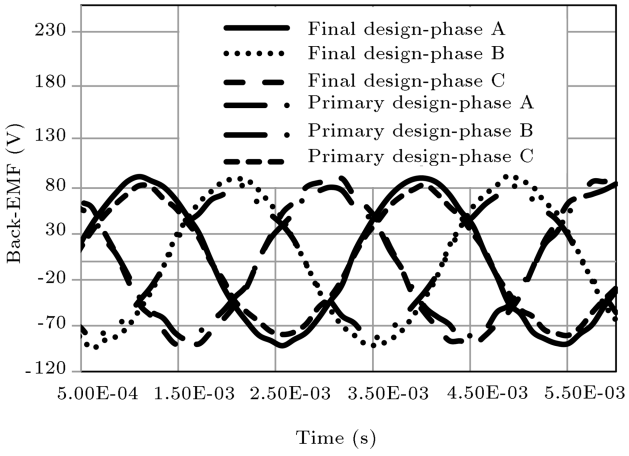

Figure 10. Three-phase back EMF at rated speed.

Figure 12. Assembled motor.

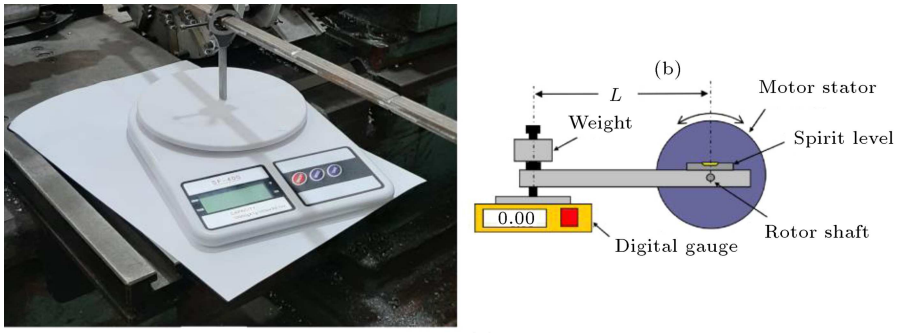

(a)

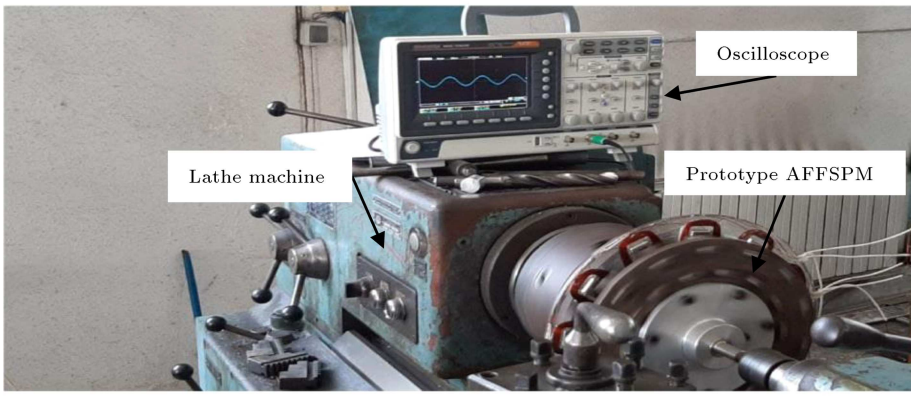

(b)

Figure 13. Schematic of the No load test setups: (a) Cogging torque test setup and (b) Back-EMF test setup.

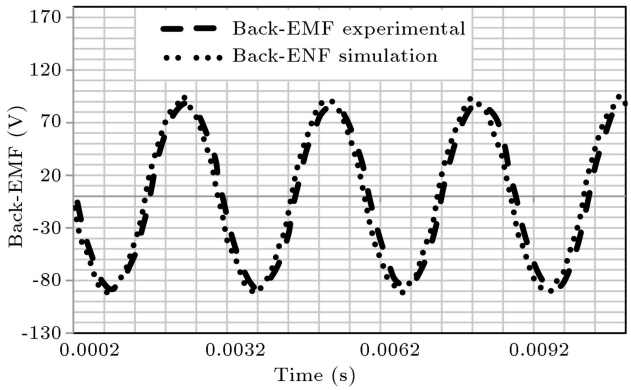

Figure 14. Phase voltage of AFFSPM motor: simulated and experimental results.

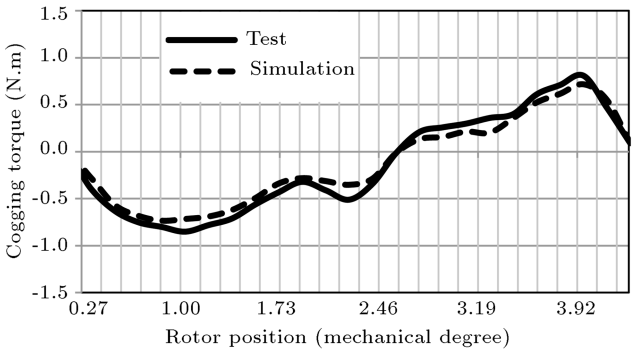

Figure 15. Cogging torque of AFFSPM motor: Simulated and experimental results.

both sides and the motor windings were connected to the oscilloscope. In this case, motor windings were of open-circuit type; therefore, the oscilloscope indicates the resulting voltage of Back-EMF. The no-load voltages measured and calculated via the FEM and cogging torque are shown in Figures 14 and 15, respectively. Comparison between the obtained results and FEM results shows that the no-load voltage and cogging torque are highly similar.

5. Conclusion

This study aimed to provide the analytical design, optimization, and simulation of a new Axial Field Flux-Switching Permanent Magnet (AFFSPM) motor with coreless stator and double rotor using Finite Element Method (FEM), as well as its construction. First, the motor was designed considering the rated values, and some dimensional and electrical characteristics of the motor were extracted. Then, the designed motor was optimized using the Taguchi algorithm aiming to minimize the cogging torque. The Three-Dimensional (3D) FEM model of the optimized model was simulated, and the initial motor and performance parameters such as the air gap flux density, torque, and Back-EMF, were compared. The optimization results showed that the optimized motor had lower cogging

torque, higher torque, and a higher Back-EMF value, compared to the primary structure. Finally, the motor was constructed and tested; the obtained results were then compared with those evaluated in the simulation section, indicating that the experimental results were largely consistent with the analytical results.

References

1. Jilong, Z., Xiaowei, Q., Xiangdong, S., et al. "Design of a novel axial flux rotor consequent-pole permanent magnet machine", *IEEE Trans. Appl. Supercond.*, **30**(4), pp. 1–6 (2020).
2. Jian, L., Yang, L., Yun-Hyun, C., et al. "Design, analysis, and prototyping of a water-cooled axial-flux permanent-magnet machine for large-power direct-driven applications", *IEEE Trans. Ind. Appl.*, **55**(4), pp. 3555–3565 (2019).
3. Youhua, W., Jiawei, L., Chengcheng, L., et al. "Development of a high-performance axial flux PM machine with SMC cores for electric vehicle application", *IEEE Trans. Magn.*, **55**(7), pp. 1–4 (2019).
4. Jilong, Z., Xiaowei, Q., and Mingyao, L. "Model predictive torque control of a hybrid excited axial field flux-switching permanent magnet machine", *IEEE Access*, **8**, pp. 33703–33712 (2020).
5. Wei, Z., Zexian, Y., Liangguan, Z., et al. "Speed sensorless control of hybrid excitation axial field flux-switching permanent-magnet machine based on model reference adaptive system", *IEEE Access*, **8**, pp. 22013–22024 (2020).
6. Kostas, L., Alexandros, M., Ilias, K., et al. "Acoustic noise of axial flux permanent magnet generators in locally manufactured small wind turbines", *IET Renew. Power Gener.*, **13**(15), pp. 2922–2928 (2019).
7. Nasrudin, A.R., Hew Wooi, P., and Mohammad Faridun Naim, T. "Design of an in-wheel axial flux brushless DC motor for electric vehicle", In *2006 International Forum on Strategic Technology*, pp. 16–19 (2006).
8. Wasiq, U., Faisal, K., Erwan, S., et al. "Torque characteristics of high torque density partitioned PM consequent pole flux switching machines with flux barriers", *CES Trans. Electr. Mach. Syst.*, **4**(2), pp. 130–141 (2020).
9. Ju Hyung, K., Yingjie, L., and Bulent, S. "Sizing, analysis, and verification of axial flux-switching permanent magnet machine", *IEEE Trans. Ind. Appl.*, **55**(4), pp. 3512–3521 (2019).
10. Ju Hyung, K., Yingjie, L., Emrah, C., et al. "Influence of rotor tooth shaping on cogging torque of axial flux-switching permanent magnet machine", *IEEE Trans. Ind. Appl.*, **55**(2), pp. 1290–1298 (2018).
11. Ranjit, K.R., *A Rimer on the Taguchi Method*, Society of Manufacturing Engineers (2010).
12. Chang-Chou, H., San-Shan, H., Cheng-Tsung, L., et al. "Optimal design of a high speed SPM motor for machine tool applications", *IEEE Trans. Magn.*, **50**(1), pp. 1–4 (2013).
13. Teck-Seng, L., Shixin, C., and Xianke, G. "Robust torque optimization for BLDC spindle motors", *IEEE Trans. Ind. Electron.*, **48**(3), pp. 656–663 (2001).
14. Huimin, W., Shu, L., Shuang, W., et al. "Optimal design of permanent magnet structure to reduce unbalanced magnetic pull in surface-mounted permanent-magnet motors", *IEEE Access*, **8**, pp. 77811–77819 (2020).
15. Sujin, L., Kyuseob, K., Sugil, C., et al. "Optimal design of interior permanent magnet synchronous motor considering the manufacturing tolerances using Taguchi robust design", *IET Electr. Power Appl.*, **8**(1), pp. 23–28 (2014).
16. Albert Johan, S., Rong-Jie, W., and Andries, J.G. "Multiobjective design of a line-start PM motor using the Taguchi method", *IEEE Trans. Ind. Appl.*, **54**(5), pp. 4167–4176 (2018).
17. Yen-Shin, L., Juo-Chiun, L., and Jennshing Jersey, W. "Direct torque control induction motor drives with self-commissioning based on Taguchi methodology", *IEEE Trans. Power Electron.*, **15**(6), pp. 1065–1071 (2000).
18. Wenju, Y., Hao, C., Xuekun, L., et al. "Design and multi-objective optimisation of switched reluctance machine with iron loss", *IET Electr. Power Appl.*, **13**(4), pp. 435–444 (2019).
19. Ji, Z., Li, H., Chen. Z., et al. "Design and optimization of permanent magnet assisted synchronous reluctance motor for better torque performance", In *2019 22nd International Conference on Electrical Machines and Systems (ICEMS)*, pp. 1–4 (2019).
20. Wenshuai, Z., Xuzhen. H., and Tianpeng, J. "Design of tubular permanent magnet synchronous linear motor in a wide temperature range environment by Taguchi-fuzzy method", In *2019 22nd International Conference on Electrical Machines and Systems (ICEMS)*, pp. 1–5 (2019).
21. Juncai, S., Fei, D., Jiwen, Z., et al. "Optimal design of permanent magnet linear synchronous motors based on Taguchi method", *IET Electr. Power Appl.*, **11**(1), pp. 41–48 (2017).
22. Hyung Jin, S., Rod, B., Zhongyi, G., et al. "Design of a 12-MW HTS wind power generator including a flux pump exciter", *IEEE Trans. Appl. Supercond.*, **26**(3), pp. 1–5 (2016).
23. Surong, H., Jian, L., Franco, L., et al. "A comparison of power density for axial flux machines based on general purpose sizing equations", *IEEE Trans. Energy Convers.*, **14**(2), pp. 185–192 (1999).

24. Jacek, F.G., Rong-Jie, W., and Maarten, J.K., *Axial Flux Permanent Magnet Brushless Machines*, Springer Science & Business Media (2008).

25. Maarten, J.K., Rong-Jie, W., and Francois, G.R. "Analysis and performance evaluation of axial flux air-cored stator permanent magnet machine with concentrated coils", In *2007 IEEE International Electric Machines & Drives Conference*, **1**, pp. 13–20 (2007).

26. Kostas, L., Katerina, T., Thomas. P., et al. "Design of axial flux permanent magnet generators using various magnetic materials in locally manufactured small wind turbines", In *2016 XXII International Conference on Electrical Machines (ICEM)*, pp. 1545–1551 (2016).

27. Maarten, J.K., Rong-Jie, W., and Francois, G.R. "Analysis and performance of axial flux permanent-magnet machine with air-cored nonoverlapping concentrated stator windings", *IEEE Trans. Ind. Appl.*, **44**(5), pp. 1495–1504 (2008).

28. Zhu, Z.Q. "A simple method for measuring cogging torque in permanent magnet machines", In *2009 IEEE Power & Energy Society General Meeting*, pp. 1–4 (2009).

Biography

Hossein Asgharpour-Alamdari received the PhD from Semnan University, Iran in 2017. He is currently an Assistant Professor at Technical and Vocational University (TVU), Babol branch, Iran. His research interests are power system stability and control, power system protection, and electrical machines and their application in renewable energy.